ISBN: 978-3-95450-253-0 ISSN: 2673-5571 doi:10.18429/JACoW-HB2023-THC2I2

EXTRACTION OF LHC BEAM PARAMETERS FROM SCHOTTKY SIGNALS

K. Lasocha*, D. Alves, C. Lannoy[1], N. Mounet, CERN, Geneva, Switzerland
T. Pieloni, EPFL, Lausanne, Switzerland
[1]also at EPFL, Lausanne, Switzerland

Abstract

Analysis of Schottky signals provides rich insights into the dynamics of a hadron beam, with well-established methods of deriving the betatron tune and machine chromaticity. In this contribution, we will report on recent developments in the analysis and understanding of the signals measured at the Large Hadron Collider during proton and Pb^{82+} fills. A fitting-based technique, where the measured spectra are iteratively compared with theoretical predictions, will be presented and compared with the previous methods. As a step beyond the classical theory of Schottky spectra, certain signal modifications due to the activity of the LHC machine systems will be discussed from the perspective of the applicability of the modified signal to the beam diagnostics.

INTRODUCTION

Schottky signals, that is fluctuations of the macroscopic beam characteristics due to the discrete motion of individual particles, can provide rich insights into their dynamics within the bunch. After the pioneering works of Simon van der Meer [1] and the first experimental observations at the Intersecting Storage Ring [2], Schottky signals have been used at many facilities as a source of information on the betatron tune, momentum spread, transverse emittance and chromaticity.

In the LHC the Schottky monitor was commissioned in 2011 [3] and underwent a major redesign during 2014-2015 [4]. Although the quality of the measured spectra during the Pb^{82+} runs is in general very good, for proton beams this is not the case. The signal is particularly difficult to analyze due to the presence of numerous coherent spectral components, enhanced by the high intensity of the proton beams.

The aim of this contribution is to summarize the recent progress in the analysis of LHC Schottky spectra. As described in Refs. [5–7], a new technique was developed, which allows for longitudinal and transverse beam parameter estimation by iterative simulation of fragments of the spectrum. A thorough revision of the theory describing Schottky signals resulted in a formal derivation of certain results, which were previously based mostly on empirical arguments. Finally, the analysis of the spectra acquired during LHC Runs 2 (2015-2018) and 3 (2022) allowed us to understand how various beam and machine conditions, not included in the theory of Schottky spectra, affect the beam.

* kacper.lasocha@cern.ch

LONGITUDINAL SCHOTTKY SIGNALS

Let us consider a single particle i, performing synchrotron oscillations around the ideal synchronous particle that travels around the synchrotron ring with angular frequency ω_0. We shall assume that the synchrotron motion is sinusoidal and that the time delay between particle i and the synchronous particle at a given location in the ring is given by:

$$\tau_i(t) = \widehat{\tau}_i \sin\left(\Omega_{s_i} t + \varphi_{s_i}\right),$$

with synchrotron frequency Ω_{s_i}, time amplitude $\widehat{\tau}_i$ and phase φ_{s_i}. The synchrotron frequency is related to the amplitude as predicted by the theory of the mathematical pendulum [8]:

$$\Omega_s = \frac{\pi}{2\mathcal{K}\left[\sin\left(\frac{h_{RF}\omega_0\widehat{\tau}}{2}\right)\right]}\Omega_{s_0}, \quad (1)$$

where Ω_{s_0} is the nominal synchrotron frequency, $h_{RF}\omega_0$ is the angular RF frequency and $\mathcal{K}$ denotes the complete elliptic integral of the first kind [9, p. 590].

At a given location in the ring, the current of a single particle i can be described, up to a scaling factor, in the following way [10]:

$$I_i(t) \propto \sum_{n=-\infty}^{\infty}\sum_{p=-\infty}^{\infty} J_p(n\omega_0\widehat{\tau}_i)e^{j([n\omega_0+p\Omega_{s_i}]t+p\varphi_{s_i})}, \quad (2)$$

where J_p denotes the Bessel function of the first kind.

The Power Spectral Density (PSD) of such a signal, as visible in Fig. 1, consists of a series of so-called synchrotron lines, symmetrically located around each harmonic of the revolution frequency ω_0. The distance between consecutive satellites is equal to the particle's synchrotron frequency.

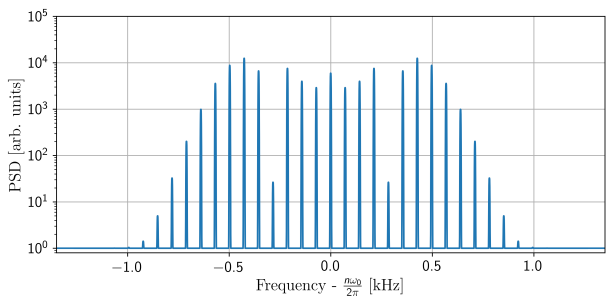

Figure 1: Simulated single particle longitudinal LHC Schottky spectrum.

The intensity signal of the whole bunch will preserve a similar structure but with a few significant differences.

ISBN: 978-3-95450-253-0 ISSN: 2673-5571 doi:10.18429/JACoW-HB2023-THC2I2

Individual particles differ with regard to their synchrotron amplitudes and frequencies. As a result, synchrotron satellites spread into wider bands. As can be seen in Fig. 2, they have a triangular shape with sub-peaks, corresponding to the combined effect of the distribution of synchrotron frequencies and the extrema of the respective Bessel functions. The relative power of synchrotron satellites changes as well. Assuming that the synchrotron phases φ_{s_i} are independent and uniformly distributed, the central $p = 0$ harmonic has significantly larger power than all the other ones. The reason behind this is twofold. Due to lack of $p\Omega_{s_i}$ term in Eq. (2) the whole power of the $p = 0$ satellite is localized in a narrow frequency range. In addition, the random phase component $p\varphi_{s_i}$ does not enter into the exponent of the term corresponding to the central satellite. As a result, at low harmonics of the revolution frequency, these terms add up coherently and the cumulative power is proportional to the square of the bunch intensity, whereas the power of other satellites is proportional only to the intensity [11].

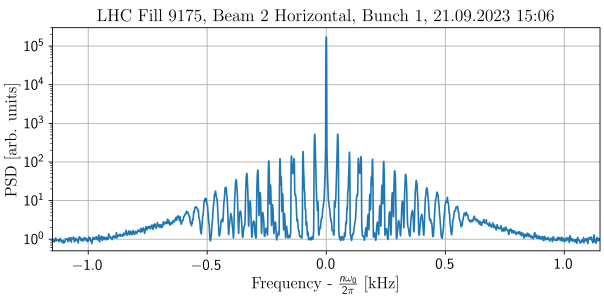

Figure 2: Longitudinal LHC Schottky spectrum.

In Fig. 3 we can see an example of a situation in which the particles' synchrotron motion is to some extent coherent. Immediately following the longitudinal blowup [12], the power of most of the satellites increases significantly. As time passes, and the filamentation of the longitudinal phase space progresses, the coherency gradually weakens. The satellites mostly affected by coherence effects are the central ones, due to the low integer multiple of the phase factor $p\varphi_{s_i}$.

TRANSVERSE SCHOTTKY SIGNALS

Let us now assume that, in addition to the longitudinal motion, the particle also performs betatron oscillations, with the resulting transverse displacement given by

$$x_i(t) = \widehat{x_i} \cos\left[\phi_{\beta_i}(t)\right],$$

where $\widehat{x_i}$ is the amplitude of the betatron motion, and the phase term is given by

$$\phi_{\beta_i}(t) = Q\omega_0 t + \frac{\widehat{Q_i}\omega_0}{\Omega_{s_i}} \sin\left(\Omega_{s_i} t + \varphi_{s_i}\right) + \varphi_{\beta_i}. \quad (3)$$

The first term of Eq. (3) corresponds to the nominal betatron tune Q, the second introduces a tune modulation due to chromaticity, and the last one is an initial betatron phase φ_{β_i}.

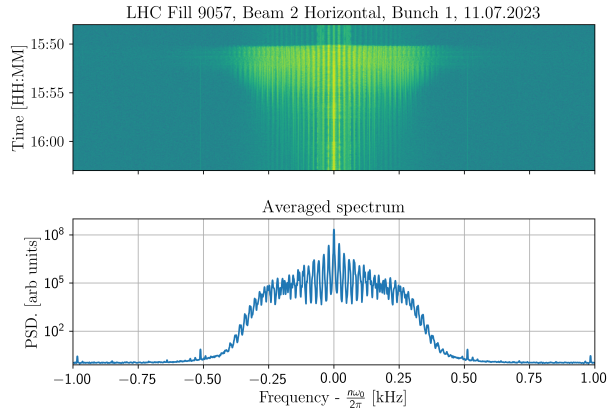

Figure 3: Effect of longitudinal blowup on Schottky spectrum. Above: spectrogram. Below: averaged spectrum.

As a result of the betatron motion, two additional spectral structures emerge in the Schottky signal. These are described, up to a scaling factor, by [6]:

$$T_i^{\pm}(t) \propto \sum_{n,p=-\infty}^{\infty} J_p\left(\chi^{\pm}_{\widehat{\tau}_i, n\mp Q_I}\right) e^{j\left(\left[(n\pm Q_F)\omega_0 + p\Omega_{s_i}\right]t + \varphi_{\beta_i} + p\varphi_{s_i}\right)}, \quad (4)$$

with

$$\chi^{\pm}_{\widehat{\tau}_i, n} = \left(n\widehat{\tau_i} \pm \frac{\widehat{Q_i}}{\Omega_{s_i}}\right)\omega_0 = (n\eta \pm Q\xi)\frac{\omega_0 \widehat{p_i}}{\Omega_{s_i} p_0},$$

where η is the slip factor, $\widehat{p_i}/p_0$ is the relative momentum deviation of particle i, and Q_I, Q_F denote the integer and fractional tune respectively.

The PSD of the so-called transverse sidebands, as can be observed in Fig. 4, consists of two spectral clusters, shifted with respect to the longitudinal band by a distance corresponding to the betatron frequency. Both bands resemble the PSD of the longitudinal intensity signal. An important difference is that, as individual particles perform betatron oscillation in an independent way, the additional betatron phase component φ_{β_i} introduces incoherence and reduces the power of the central satellite. In addition, for non-zero chromaticity the argument of the Bessel function is different for both bands which leads to a different band shape.

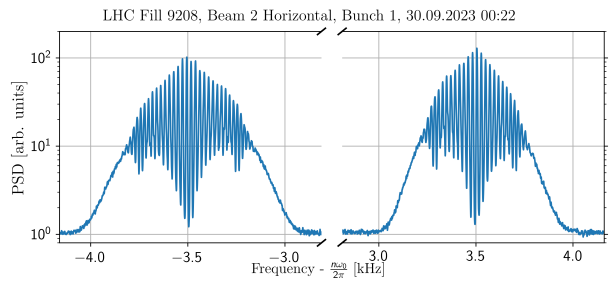

Figure 4: Transverse Schottky spectrum.

ISBN: 978-3-95450-253-0 ISSN: 2673-5571 doi:10.18429/JACoW-HB2023-THC2I2

MATRIX FORMALISM

As shown in Refs. [5, 6], assuming no coherence in the betatron nor synchrotron motion and excluding the central longitudinal synchrotron satellite, the PSD of multiparticle Schottky signal is equal to the sum of single particle PSDs.

For the longitudinal Schottky spectrum around the selected harmonic n of the revolution frequency, we have:

$$P(\omega) \propto \sum_{i=1}^{N} \sum_{p=-\infty}^{\infty} J_p^2\left(n\omega_0\widehat{\tau}_i\right)\delta(\omega - n\omega_0 - p\Omega_{s_i}),$$

where $\delta(\cdot)$ is a Dirac delta and N is the number of particles.

The PSD of the transverse Schottky signals is described by the expression:

$$P_T^{\pm}(\omega) = \widehat{x}\sum_{i=1}^{N} P_T^{\pm}(\omega, \widehat{\tau}_i),$$

where $\widehat{x}$ is a common scaling factor, resulting from the assumption that the amplitudes of betatron and synchrotron motion are independent quantities, while $P_T^{\pm}(\omega, \widehat{\tau}_i)$ is the single particle contribution given by

$$P_T^{\pm}(\omega, \widehat{\tau}_i) = \sum_{p=-\infty}^{\infty} J_p^2\left(\chi^{\pm}_{\widehat{\tau}_i, h\mp Q_I}\right)\delta[\omega-(h\pm Q_F)\omega_0-p\Omega_s(\widehat{\tau}_i)].$$

Analyzing the expressions above, one can note that the only quantities specific to individual particles are Ω_{s_i} and $\widehat{\tau}_i$. In addition, according to Eq. (1), there is a one-to-one relationship between these quantities. The only other parameters needed to uniquely determine the Schottky spectrum are the betatron tune Q, the nominal synchrotron frequency Ω_{s_0}, and the chromaticity $Q\xi$. Taking the discrete distribution of synchrotron amplitudes $g(\widehat{\tau}_j)$ among all the particles, and assuming that the single particle contributions add up incoherently at all considered frequencies, one can write the Discrete Fourier Transform (DFT) of the total multiparticle Schottky signals P_{DFT} and $P^{T,\pm}_{DFT}$ in matrix form:

$$\underbrace{\begin{bmatrix} P_{DFT}(\omega_1, \widehat{\tau}_1, \Omega_{s_0}) & \cdots & P_{DFT}(\omega_1, \widehat{\tau}_n, \Omega_{s_0}) \\ P_{DFT}(\omega_2, \widehat{\tau}_1, \Omega_{s_0}) & \cdots & P_{DFT}(\omega_2, \widehat{\tau}_n, \Omega_{s_0}) \\ \vdots & \ddots & \vdots \\ P_{DFT}(\omega_m, \widehat{\tau}_1, \Omega_{s_0}) & \cdots & P_{DFT}(\omega_m, \widehat{\tau}_n, \Omega_{s_0}) \end{bmatrix}}_{\mathcal{M}(\Omega_{s_0})} \cdot \underbrace{\begin{bmatrix} \widetilde{g}(\widehat{\tau}_1) \\ \widetilde{g}(\widehat{\tau}_2) \\ \vdots \\ \widetilde{g}(\widehat{\tau}_n) \end{bmatrix}}_{\mathcal{A}} = \underbrace{\begin{bmatrix} P_{DFT}(\omega_1) \\ P_{DFT}(\omega_2) \\ \vdots \\ P_{DFT}(\omega_m) \end{bmatrix}}_{P_{DFT}}, \tag{5}$$

and

$$\underbrace{\begin{bmatrix} P^{T,\pm}_{DFT}(\omega_1, \widehat{\tau}_1, \Omega_{s_0}, Q, Q\xi) & \cdots & P^{T,\pm}_{DFT}(\omega_1, \widehat{\tau}_n, \Omega_{s_0}, Q, Q\xi) \\ P^{T,\pm}_{DFT}(\omega_2, \widehat{\tau}_1, \Omega_{s_0}, Q, Q\xi) & \cdots & P^{T,\pm}_{DFT}(\omega_2, \widehat{\tau}_n, \Omega_{s_0}, Q, Q\xi) \\ \vdots & \ddots & \vdots \\ P^{T,\pm}_{DFT}(\omega_m, \widehat{\tau}_1, \Omega_{s_0}, Q, Q\xi) & \cdots & P^{T,\pm}_{DFT}(\omega_m, \widehat{\tau}_n, \Omega_{s_0}, Q, Q\xi) \end{bmatrix}}_{\mathcal{M}(\Omega_{s_0}, Q, Q\xi)} \cdot \underbrace{\begin{bmatrix} \widetilde{g}(\widehat{\tau}_1) \\ \widetilde{g}(\widehat{\tau}_2) \\ \vdots \\ \widetilde{g}(\widehat{\tau}_n) \end{bmatrix}}_{\mathcal{A}} = \underbrace{\begin{bmatrix} P^{T,\pm}_{DFT}(\omega_1) \\ P^{T,\pm}_{DFT}(\omega_2) \\ \vdots \\ P^{T,\pm}_{DFT}(\omega_m) \end{bmatrix}}_{P^{T,\pm}_{DFT}}, \tag{6}$$

where the single particle DFTs $P_{DFT}(\omega_i, \widehat{\tau}_j, \Omega_{s_0})$ and $P^{T,\pm}_{DFT}(\omega_i, \widehat{\tau}_j, \Omega_{s_0}, Q, Q\xi)$ can be calculated directly from Eqs. (2) and (4).

The number of considered amplitudes $\widehat{\tau}_1, \ldots, \widehat{\tau}_n$ is a tradeoff between the time-complexity and discretisation error. For the analysis of the LHC Schottky spectra it was chosen to take 50 amplitudes uniformly distributed over the whole RF bucket.

SCHOTTKY SIGNALS IN THE LHC

The LHC Schottky monitors [4] probe the beam field using four pairs of symmetrically arranged, approximately 1 m long slotted waveguides, one pair per beam and per plane. These pickups are sensitive to the beam field in approximately a 200 MHz bandwidth around the central frequency of 4.81 GHz. The choice of this frequency is a tradeoff between minimizing the strength of the central longitudinal satellite and having a measurable width of longitudinal and transverse sidebands while ensuring no overlap between them. Additional suppression of the strong longitudinal signal is obtained by subtracting the outputs of both waveguides with the use of a hybrid. The fast gate-switch enables observation of any selected subset of bunches. During standard operation single bunches are observed. After gating, the bunch signal is sequentially filtered and downconverted, so that the final digitized output is essentially a 15 kHz slice of the original spectrum around the $427725 \times \omega_0/2\pi \approx 4.81$ GHz, mixed down to the LHC revolution frequency $\omega_0/2\pi \approx 11.2455$ kHz.

The sampling frequency, locked to the RF frequency to avoid drifts during ramps and orbit corrections, is set to $4 \times \omega_0/2\pi$. The DFT of the last $2^{16} = 65536$ points is cal-

ISBN: 978-3-95450-253-0 ISSN: 2673-5571 doi:10.18429/JACoW-HB2023-THC2I2

culated every second, what results in the spectral resolution of approximately 0.69 Hz.

Although the LHC Schottky system is by design a transverse monitor, imperfections of the delta hybrid as well as the very strong intensity signal lead to the inevitable presence of the longitudinal band next to the measured transverse sidebands.

As discussed in Ref. [11], the theory of Schottky spectra presented in the previous sections describes only an expected, probability space-averaged power of Schottky signals. This can be approximated with time-averaged instantaneous spectra. To analyze LHC Schottky spectra, a simple moving average of consecutive 100 spectra is taken.

SPECTRA FITTING PROCEDURE

The main benefit of the matrix formalism, described by Eqs. (5) and (6), is the fact that it allows for the efficient simulation of Schottky signals without the need of performing time-consuming and Monte-Carlo-based multiparticle simulations. In this way the impact of different beam parameters on Schottky spectra can be studied and visualised.

From the perspective of beam diagnostics, one can adopt the complementary approach, i. e., given a measured Schottky spectrum P^{exp}_{DFT}, one can look for a set of beam and machine parameters that allows to reproduce the measurement. To achieve that, we define a cost function:

$$C(\Omega_{s_0}, \mathcal{A}, Q, Q\xi) = |\mathcal{M}(\Omega_{s_0}, Q, Q\xi) \cdot \mathcal{A} - P^{exp}_{DFT}|^2, \quad (7)$$

where $|\cdot|$ denotes the standard Euclidean norm. The cost function expresses a distance between the simulated spectrum, and the measured one. To minimize it, one can employ an optimizing routine, such as the L-BFGS-B [13] or a differential evolution algorithm [14].

The number of arguments in the cost function, and therefore the number of parameters determined in the optimizing procedure, can vary. For example, when analyzing the longitudinal part of the Schottky spectra, one does not take the betatron tune and the chromaticity into account. In addition, if certain parameters are already known in advance (e. g. measured directly or indirectly with another instrument), they can be used in the cost function as constant parameters, reducing the number of variables to be determined.

In principle, the synchrotron amplitude distribution $\mathcal{A}$, being a distribution, consists of a bigger number of independent parameters. As previously discussed, in the case of the LHC we consider a discrete 50-point distribution. To reduce this number of free parameters, a regularisation of the synchrotron amplitude distribution is taken. Based on experimental observations, it is assumed that the synchrotron amplitude distribution follows the Rice distribution [15] and therefore is described by only two parameters.

One of the best features of the matrix-based spectrum fitting procedure is the fact that it imposes no restrictions on the frequencies taken in Eqs. (5) and (6). If for some reason, e. g. due to the local distortions of the Schottky spectrum, it is desired to exclude certain frequencies from the analysis, one can freely do so.

SYNCHROTRON FREQUENCY

The nominal synchrotron frequency is a parameter which in principle can be calculated with a simple formula [16]:

$$\Omega_{s_0} = \sqrt{\frac{q h_{RF} \omega_0 \eta \hat{V} \cos(\phi_s)}{2\pi R p_0}}, \quad (8)$$

where q is the particle charge, $\hat{V}$ is the RF voltage, ϕ_s is the RF phase of the synchronous particle and R is the radius of the synchrotron ring.

If, however, some beam and machine parameters appearing in Eq. (8) are known only with a limited precision, as is the case for the effective LHC RF voltage and slip factor [17], these uncertainties will propagate to the estimate of the nominal synchrotron frequency.

An alternative way to calculate the nominal synchrotron frequency is to analyze the longitudinal Schottky spectrum. As discussed previously, the synchrotron frequency is reflected in the distance between the following Bessel satellites of the longitudinal and transverse sidebands. Having an experimental Schottky spectrum, the spectrum fitting procedure based on minimization of the cost function

$$C(\Omega_{s_0}, \mathcal{A}) = |\tilde{\mathcal{M}}(\Omega_{s_0}) \cdot \mathcal{A} - P^{exp}_{DFT}|^2 \quad (9)$$

determines the simulation parameters that most closely match the measurement. The results of such minimization, using a differential evolution algorithm, are presented in Fig. 5.

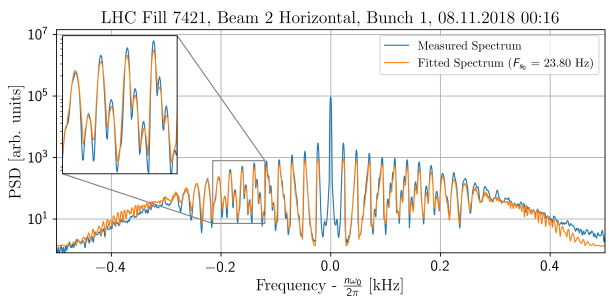

Figure 5: Measured and fitted longitudinal Schottky spectra.

As will be explained in the next section, for the overwhelming majority of the time during standard LHC operation, the synchrotron amplitude distribution can be calculated based on the longitudinal bunch profile. In such a case, the nominal synchrotron frequency is the only parameter that needs to be determined in Eq. (9), and potentially time-consuming minimizing routines can be replaced with a simple scan over the plausible values of the synchrotron frequency.

LONGITUDINAL BUNCH PROFILES

Under stationary conditions, assuming a uniform distribution of synchrotron phases among the particles, the syn-

ISBN: 978-3-95450-253-0 ISSN: 2673-5571 doi:10.18429/JACoW-HB2023-THC2I2

chrotron amplitude distribution $g(\widehat{\tau})$ is related to the longitudinal bunch profile $\mathcal{B}(\tau)$ by the following expression [5]:

$$\mathcal{B}(\tau) = \int_{|\tau|}^{\infty} \frac{g(\widehat{\tau})}{\pi\sqrt{\widehat{\tau}^2 - \tau^2}} \mathrm{d}\widehat{\tau}. \tag{10}$$

As a consequence, determining the synchrotron amplitude distribution, for example by minimizing the cost function (Eq. (9)), is equivalent to deriving the longitudinal bunch profile.

An example of such a measurement is presented in Fig. 6 where synchrotron amplitude distributions, determined with a fitting procedure, were subsequently transformed into corresponding bunch profiles according to Eq. (10). As the same longitudinal profile should be derived from both vertical and horizontal Schottky monitors, estimates based on both devices were compared with the independent measurement with the Wall Current Monitor (WCM) [18].

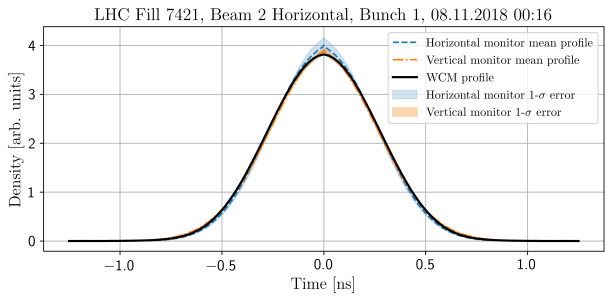

Figure 6: Longitudinal bunch profiles measured with WCM and estimated based on Schottky spectra. Averages and 1-σ error margins taken over a time interval of 100 seconds.

BETATRON TUNE

The measurements of the betatron tune are based on the analysis of the transverse parts of the spectrum. The theory predicts that the distance between the central satellites in the two transverse sidebands will be equal to $2Q_F\omega_0$. The determination of the central satellites can be achieved using the *Mirrored Difference* (MD) algorithm, which is based on the fact that the central satellite is the axis of symmetry of the whole sideband. All frequency bins of the sideband are scanned, and in each bin the following cost function is calculated:

$$C_{MD}(k) = \sum_{i=1}^{i=M} \left| P_T^{\pm}(\omega_{k-i}) - P_T^{\pm}(\omega_{k+i}) \right|,$$

where M is a predefined constant. The value of k which minimizes the cost function corresponds to the frequency bin of the sideband center. In case a higher tune resolution is desired, values between the frequency bins can be interpolated.

An example of the tune derived in such a way is presented in Fig. 7. As we can see, the MD algorithm can be used to derive betatron tunes of individual bunches with a precision higher than 10^{-4}.

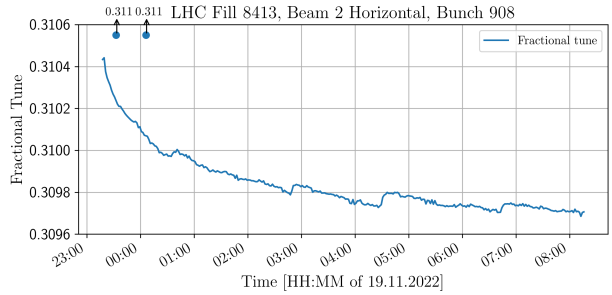

Figure 7: Betatron tune estimated using MD algorithm.

CHROMATICITY

Whereas all previously mentioned beam characteristics can also be derived using other LHC diagnostic instruments, Schottky signal analysis remains the only technique with a potential for non-invasive measurements of chromaticity at high beam energies and intensities.

The information on the chromaticity is imprinted in the differences between the widths of transverse Schottky sidebands. It can be shown [6] that, in LHC conditions, and if one takes $\Delta f_{\pm}$ to be the root-mean-square (RMS) width of respectively the upper (+) and lower (-) transverse sidebands, the chromaticity is given by the following expression:

$$Q\xi = -\eta \left(n \frac{\Delta f_- - \Delta f_+}{\Delta f_- + \Delta f_+} - Q_I \right). \tag{11}$$

Estimating chromaticity using Eq. (11) is only possible in stationary conditions, i. e., whenever particle motion is purely incoherent. In the presence of local spectrum distortions, induced e. g. due to the residual coherent intra-bunch motion, Eq. (11) cannot be directly used. In these cases the modified shape of the sidebands affects the RMS width estimation and deteriorates the chromaticity estimate. In these cases, the spectrum fitting procedure can be applied. As previously discussed, frequency bins containing local distortions can be excluded from the analysis and only the remaining frequency bins would be fitted, as shown Fig. 8.

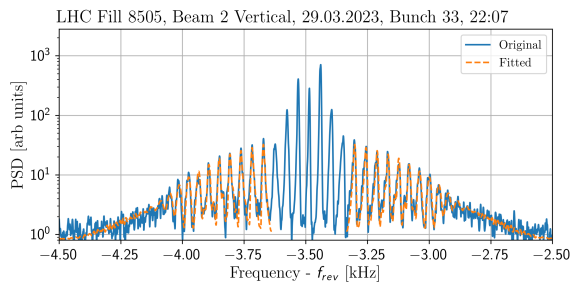

Figure 8: Measured and fitted lower transverse Schottky sideband, with coherent satellites excluded from the analysis.

The estimated values of chromaticity are shown in Fig. 9. The result is in agreement with the prior reference measurement using the invasive RF modulation technique [19],

ISBN: 978-3-95450-253-0 ISSN: 2673-5571 doi:10.18429/JACoW-HB2023-THC2I2

whereas the direct application of Eq. (11) would result in an error by over 4 units.

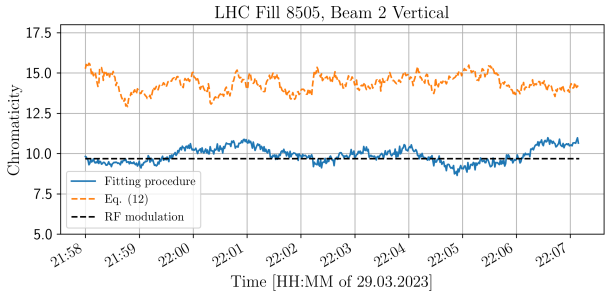

Figure 9: Results of chromaticity measurements using spectra fitting and other techniques.

The overall analysis procedure can be implemented in such a way that, by the time the transverse sidebands are to be fitted, chromaticity is the only unknown argument of the cost function (Eq. (7)). In this case, chromaticity can be estimated by scanning a grid of values, within a plausible range, and looking for the minimum of the cost function.

LIMITATIONS

The existing theory of Schottky spectra and the developed diagnostic techniques cannot be applied universally for all beam conditions. Assumptions on the form of single particle motion, the absence of betatron and synchrotron coherence, and the necessity of relatively long spectral averaging put strong limitations on the analysis potential. While the coherence in particles' motion can be often mitigated with the spectra fitting procedure, other conditions prevent the Schottky signals acquired during the big part of the LHC operation from being analyzed with the discussed techniques.

Foremost, the averaged Schottky spectra remain obscure when beam and machine parameters change. This problem can be illustrated by the tune shift example shown in Fig. 10. As the spectrogram remains readable, the application of image recognition algorithms, that take the whole spectogram as input, might be a good mitigation technique.

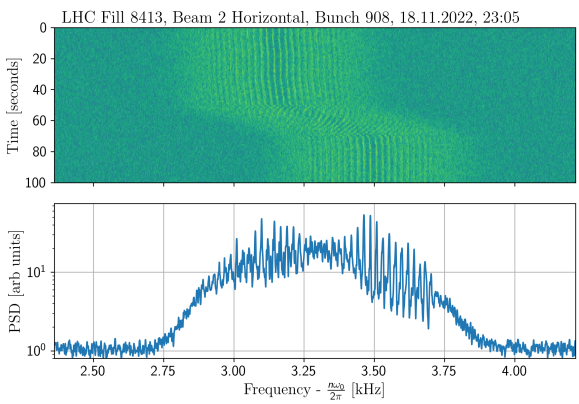

Figure 10: Spectrogram and averaged Schottky spectrum during the tune shift.

Another limitation is the presence of conditions that are not yet described by the theory of Schottky spectra. A prominent example is the effect of octupoles, acting on the beam during most LHC fills, shown in Fig. 11. Unless the octupole current is small compared to the beam energy, transverse satellites are smeared and shifted due to the convolution with the octupole-induced betatron tune spread.

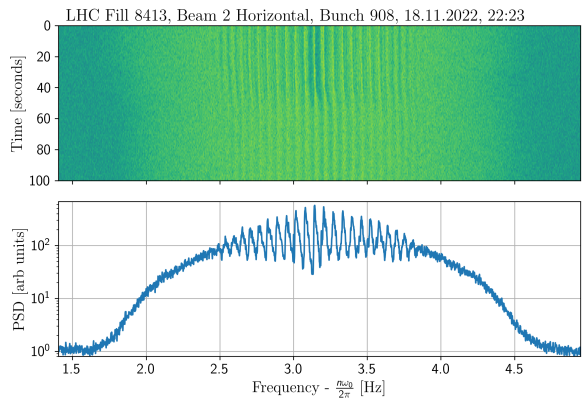

Figure 11: Spectrogram and averaged Schottky spectrum during the octupole magnet ramp.

CONCLUSION

Recent developments in the understanding and analysis of the LHC Schottky spectra have shown their potential to estimate a rich variety of beam and machine characteristics. At the same time, due to the high sensitivity of Schottky signals, individual parameters can be hard to extract from the observed spectra, especially if the particles' dynamics are governed by effects not included in the so-far developed theory.

Within the next days, Schottky spectra of both planes and both LHC beams will start being acquired and analyzed continuously. The analysis pipeline begins with longitudinal profiles being acquired by the WCM system and transformed into a distribution of synchrotron amplitudes. Then, the synchrotron frequency is determined using the spectra fitting technique. In parallel, the MD algorithm determines the betatron tune. Finally, the chromaticity is estimated by scanning different values and finding the best match for the transverse sidebands of the spectrum. To automatically exclude frequency bins containing coherent components, it is verified if the power in a given bin is in agreement with the statistical properties of the Schottky spectra, described in Ref. [11].

Future efforts will be put towards expanding the existing theory of Schottky spectra. Due to the complexity of its analytical description, a particularly important part of this research is based on macroparticle simulations [20], with special emphasis on the beam impedance [21, 22].

REFERENCES

[1] S. van der Meer, "Stochastic damping of betatron oscillations in the ISR" CERN, Geneva, Switzerland, Rep. CERN-ISR-

ISBN: 978-3-95450-253-0 ISSN: 2673-5571 doi:10.18429/JACoW-HB2023-THC2I2

PO-72-31, 1972.
https://cds.cern.ch/record/312939

[2] J. Borer *et al.*, "Non-destructive diagnostics of coasting beams with Schottky noise", in *Proc. 9th Int. Conf. on High Energy Accelerators*, Stanford, CA, USA, May 1974, pp. 53–56. https://cds.cern.ch/record/310532

[3] F. Caspers *et al.*, "Capabilities and Performance of the LHC Schottky Monitors", in *Proc. 10th European Workshop on Beam Diagnostics and Instrumentation for Particle Accelerators*, Hamburg, Germany, May 2011, pp. 44–46. https://cds.cern.ch/record/1375163

[4] M. Betz *et al.*, "Bunched-beam Schottky monitoring in the LHC", *Nucl. Instrum. Meth. A*, vol. 874, pp. 113–126, 2017. doi:10.1016/j.nima.2017.08.045

[5] K. Lasocha and D. Alves, "Estimation of longitudinal bunch characteristics in the LHC using schottky-based diagnostics", *Phys. Rev. Accel. Beams*, vol. 23, p. 062803, 2020. doi:10.1103/PhysRevAccelBeams.23.062803

[6] K. Lasocha and D. Alves, "Estimation of transverse bunch characteristics in the lhc using schottky-based diagnostics", *Phys. Rev. Accel. Beams*, vol. 25, p 062801, 2022. doi:10.1103/PhysRevAccelBeams.25.062801

[7] K. Lasocha and D. Alves, "Analysis of the Transverse Schottky Signals in the LHC", in *Proc. IBIC'23*, Saskatoon, Canada, Sep. 2023, pp. 462–466. doi:10.18429/JACoW-IBIC2023-TH2C03

[8] K. Ochs, "A comprehensive analytical solution of the nonlinear pendulum", *Eur. J. Phys.*, vol. 32, p. 479, 2011. doi:10.1088/0143-0807/32/2/019

[9] M. Abramowitz and I. A. Stegun, *Handbook of Mathematical Functions with Formulas, Graphs, and Mathematical Tables*, 9th ed., Dover, 1964. doi:10.1119/1.15378

[10] D. Boussard, "Schottky noise and beam transfer function diagnostics", CERN, Geneva, Switzerland, CERN Accelerator School: Advanced Accelerator Physics course, 1995. doi:10.5170/CERN-1995-006.749

[11] C. Lannoy *et al.* "Statistical Properties of Schottky Spectra", in *Proc. IBIC'23*, Saskatoon, Canada, Sep. 2023, pp. 438–442. doi:10.18429/JACoW-IBIC2023-WEP035

[12] P. Baudrenghien and T. Mastoridis, "Longitudinal emittance blowup in the Large Hadron Collider", *Nucl. Instrum. Meth. A*, vol. 726, pp. 181–190, 2013. doi:10.1016/j.nima.2013.05.060

[13] R. Byrd *et al.*, "A Limited Memory Algorithm for Bound Constrained Optimization", *SIAM Journal of Scientific Computing*, vol. 16, pp. 1190–1208, 1995. doi:10.1137/0916069

[14] R. Storn and K. Price, "Differential evolution - a simple and efficient heuristic for global optimization over continuous spaces," *Journal of Global Optimization*, vol. 11, pp. 341–359, 1997. doi:10.1023/A:1008202821328

[15] A. Abdi *et al.*, "On the estimation of the K parameter for the Rice fading distribution", *IEEE Comm. Lett.*, vol. 5, pp. 92–94, 2001. doi:10.1109/4234.913150

[16] F. Tecker, "Longitudinal beam dynamics", CERN Accelerator School: Advanced Accelerator Physics Course, Trondheim, Norway, Aug. 2013. https://cds.cern.ch/record/1982417

[17] J. Keintzel, L. Malina, and R. Tomas Garcia, "Momentum Compaction Factor Measurements in the Large Hadron Collider", in *Proc. IPAC'21*, Campinas, Brazil, May 2021, pp. 1360–1363. doi:10.18429/JACoW-IPAC2021-TUPAB011

[18] G. Papotti, T. Bohl, F. Follin, and U. Wehrle, "Longitudinal Beam Measurements at the LHC: The LHC Beam Quality Monitor", in *Proc. IPAC'11*, San Sebastian, Spain, Sep. 2011, pp. 1852–1854. https://jacow.org/IPAC2011/papers/TUPZ022.pdf

[19] O. S. Brüning, W. Höfle, R. Jones, T. Linnecar, and H. Schmickler, "Chromaticity Measurements via RF Phase Modulation and Continuous Tune Tracking", in *Proc. EPAC'02*, Paris, France, Jun. 2002, pp. 1852–1854. https://jacow.org/e02/papers/THPRI061.pdf

[20] C. Lannoy, D. Alves, N. Mounet, and T. Pieloni, "LHC Schottky Spectrum from Macro-Particle Simulations", in *Proc. IBIC'22*, Kraków, Poland, Sep. 2022, pp. 308–312. doi:10.18429/JACoW-IBIC2022-TUP34

[21] C. Lannoy *et al.* "Effect of Longitudinal Beam-Coupling Impedance on the Schottky Spectrum of Bunched Beams", in *Proc. IBIC'23*, Saskatoon, Canada, Sep. 2023, pp. 433–437. doi:10.18429/JACoW-IBIC2023-WEP034

[22] C. Lannoy *et al.*, "Studies on the Effect of Beam-Coupling Impedance on Schottky Spectra of Bunched Beams", presented at HB'23, Geneva, Switzerland, Oct. 2023, paper THBP47, these proceedings.